ChemComm

Accepted Manuscript

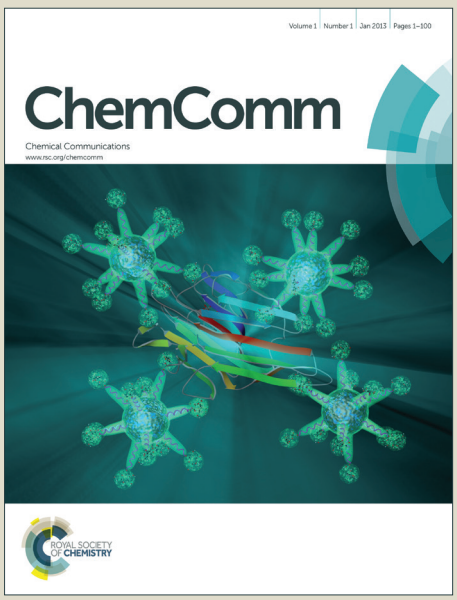

ROYAL SOCIETY OF CHEMISTRY

www.rsc.org/chemcomm

ChemComm

RSCPublishing

COMMUNICATION

Ag-Si artificial microflowers for plasmon-enhanced solar water splitting

Cite this: DOI: 10.1039/x0xx00000x

Chih-Jung Chen,[a] Ming-Guei Chen,[b] Chih Kai Chen,[a] Pin Chieh Wu,[c] Po-Tzu Chen,[c] Mrinmoyee Basu,[a] Shu-Fen Hu,*[b] Din Ping Tsai[c] and Ru-Shi Liu*[ad]

Received 00th January 2012,
Accepted 00th January 2012

DOI: 10.1039/x0xx00000x

www.rsc.org/

We prepared Ag-Si microflowers as the photocathode for water splitting through a facile chemical method. The photocurrent and hydrogen evolution rate of partially Ag particles decorated-Si microwires, were enhanced through the synergetic effects of Ag co-catalytic and plasmonic assistance.

Solar water splitting has been regarded as a potential hydrogen generation method since Fujishima and Honda first demonstrated in 1972 because of its zero carbon emission.[1] Among numerous semiconductor materials, silicon is considered as the most promising photocathode for solar fuel production because its conduction band edge (ca. -0.46 V vs. NHE) is more negative than the water reduction potential. Si nanowire (NW) or microwire (MW) arrays have given substantial interest because of its enhanced light absorption, shorter minority carrier diffusion length, and increased surface area compared to planar structures.[2] Variety of strategies like integrating different materials, co-catalyst[3], homojunction[3e, f], or heterostructure (heterojunction)[4] have been employed to improve the photoelectrochemical (PEC) efficiency of Si wires.

Recently, localized surface plasmon resonance (LSPR) has had an increasingly important function in solar and PEC cells.[5] Noble metal nanostructures generate LSPR by an incident irradiation, which corresponds to the oscillating frequency of collective surface electrons. Following plasmonic excitation in noble metals, non-irradiative decay, which involves either intraband transition within the conduction band or interband transition between the *d* band and the conduction band, generates hot electrons.[6] These hot electrons with energy levels higher than the Schottky barrier can be injected into neighbouring semiconductors to enhance the photocatalytic activity. On the other hand, the formation rates of charge carriers in a semiconductor are proportional to the local intensity of the electric field.[7] The intensity of spatially non-homogeneous fields caused by plasmonic excitation are strongest at the semiconductor-metal nanostructure interface and result in the reduced recombination. A past study has demonstrated that a higher (85%) photocurrent at +0.5 V of an Ag-embedded ZnO nanorod array was achieved through LSPR assistance and plasmon propagation, resulting in the improved capture of incident light and collection of electron-hole pairs.[8] The unsuppressed PEC performance of an embedded structure has been proposed without surface modification of the ZnO nanorods. By contrast, the Pt nanoparticles, which are uniformly decorated on a Si NW array by using atomic layer deposition (ALD) system, suffered from low ionic and gas diffusion efficiencies for the photocurrent measurement because of the rough surfaces.[3c] In the present work, we demonstrated the modification of a Si MW array by using Ag plasmonic particles as the photocathode for solar water splitting. The morphologies of the Ag-Si electrodes, which were prepared through a facile chemical method, were artificial microflowers with less surface decoration on Si roots. This preparation method was also advantageous for the prevention of Si roots from the formation of insulating oxide layer during the particles deposition process. The photocurrent and hydrogen evolution rate of partially Ag particles decorated-Si MWs, were enhanced through the synergetic effects of co-catalytic and LSPR assistance.

In this study, Si roots of microflowers were prepared through dry etching fabrication (see Fig. S1 and details in ESI). For the PEC comparison, Si MWs with various lengths were fabricated using different systems or etching time, but X-ray diffraction (XRD) and Raman spectra reveal no differences in the crystallography or surface properties (see Fig. S2, ESI). The scanning electron microscopy (SEM) images show the pitch size of pristine Si MWs was ~2 μm, and the diameter of the single wires was ~850 nm (see Fig. S3, ESI). Besides, the cross-sectional images present that the lengths of Si MWs were 1, 3 and 12 μm. No evident difference was also observed between the appearances of Si MWs prepared through different fabrication procedures. The ultraviolet-visible (UV-Vis) absorption spectra revealed that longer Si MWs had stronger absorption because the incident illumination penetrates the microstructure through multiple routes resulting in the re-absorption of reflected light and the enhancement of light trap capacity (see Fig. S4, ESI). Stronger absorption led to higher amount of electron-hole pairs for splitting water, so the longest Si MWs were selected to modify with Ag particles to further improve the PEC efficiency. The native oxide of Si MWs was first etched using diluted hydrofluoric (HF) acid and then immersed in the Ag reagent (5 mM $AgNO_3$ dissolved in 5 M HF acid solution) for specific durations. The growth mechanism of these Ag particles can be expressed as two half-reactions ($Ag^+ + e^- \rightarrow Ag$ and $Si + 6F^- \rightarrow SF_6^{2-} + 4e^-$).[9] For convenience, we abbreviated Si MWs with different Ag particles

loading amounts as "Ag-Si-T", in which T represents Ag deposition time (sec). The morphology of Ag-Si-30 was microflowers, and some of larger rod-shaped Ag particles with aspect ratios within 2 to 5 were deposited on the top caps of Si MWs (Fig. 1a-b). Smaller Ag nanospheres with diameters of 20 to 100 nm were distributed around the surface sides of Si MWs. Although portions of Si MWs were oxidized to SiF_6^{2-} ions during the Ag decoration process, there was no significant variations in the morphologies of Si roots. UV-Vis spectra revealed that Ag-Si electrodes had three dominant absorption regions (Fig. 1c). The absorption in the visible light (420-800 nm) was caused by the inherent absorption of Si MWs, whereas the absorption peak at ~380 nm was attributed to the LSPR of Ag nanostructures, which was enhanced with increasing Ag deposition time. This plasmonic absorption can also be investigated from the Ag-modified Si, which functions as a photovoltaic material in solar cells.[10] The strong absorption (below ~340 nm) was resulted from the intrinsic absorption of Ag particles. We noted that Si MWs had decreased absorption in visible light after the deposition of Ag particles. This result demonstrated that Ag nanostructures partially blocked the incident irradiation and reduced the innate absorption of underlying Si MWs. However, the absorption edge of Ag-Si electrodes extended to the UV region, which constitutes ~5% of the solar spectrum.

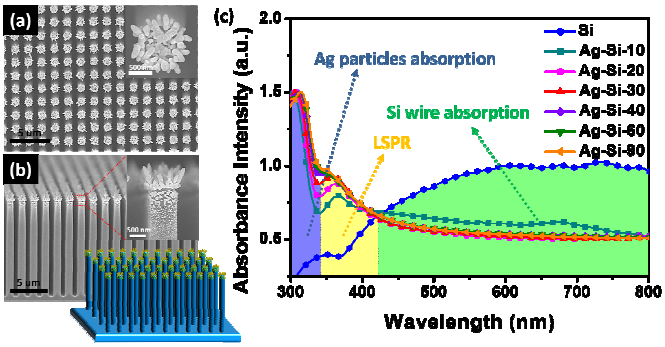

Fig. 1 (a-b) Top view and cross-sectional SEM images of Ag-Si wire array for deposition time of 30 s. (c) UV-Vis absorption spectra of Ag-Si electrodes with varied Ag deposition durations.

The three-electrode PEC cells were carried out in a 0.5 M Na_2SO_4 aqueous solution (tune to pH = 1 by the sulfuric acid) under solar illumination (100 mW/cm^2). The linear-sweep voltammograms of Si MWs with different lengths (see Fig. S5, ESI) showed that there nearly no photoresponse was observed for 1 μm long Si MWs, but Si electrode with 12 μm length had increased photoresponse and the photocurrent reached -0.13 mA/cm^2 at -1.0 V. The higher photocurrent of longer Si MWs was caused by stronger light absorption and increased surface area to react with protons in the electrolyte. Here, the longest Si MWs was immersed in diluted HF acid (abbreviated to Si-HF) to remove the native oxide, and its photocurrent increased dramatically to -5.6 mA/cm^2 at -1.0 V. This result indicates that the insulating oxide layer reduced the photogenerated carriers to migrate to the surface and increased the recombination. To further improve the PEC performance, plasmonic Ag particles were deposited on 12 μm long Si MWs. Both photocurrents and on-set potentials of Ag-decorated Si MWs were significantly enhanced compared with those of the Si-HF electrode (Fig. 2a). A ~500 mV positive shift of on-set potential (defined as the current reaching -1.0 mA/cm^2) was observed through the assistance of Ag co-catalysts, which were functioned as electron collectors, and decreased the recombination.[11] However, the on-set potentials of the Ag-Si electrodes after deposition time above 40 s were saturated at ~0.1 V vs RHE (Fig. 2b). This suggests that nearly all Ag particles are concentrated on the tips of Si MWs, thereby there is no further improvement of turn-on potentials for the longer modifying duration. This on-set potential enhancement is more substantial compared with the results in precious studies about ZnO/Si heterojunction structures.[4] The maximum photocurrent reached -35 mA/cm^2 at -1.0 V after Si MWs were deposited with Ag particles for 30 s (Ag-Si-30). Further increasing the Ag deposition amount led to the reduced photocurrent. The SEM images of Si MWs with Ag particles decoration above 40 s revealed that Ag nanostructures were cross-linked dendrites. This morphology blocked the incident light and reduced the light absorption of underlying Si MWs, and also functioned as trapping centers of photoexcited carriers for the recombination. (see Fig S6, ESI).[12]

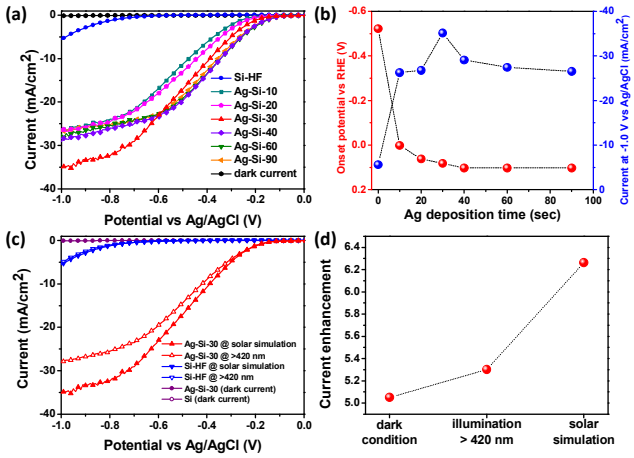

Fig. 2 (a) Linear-sweep voltammograms of Ag-Si electrodes with varying Ag deposition times. (b) On-set potential and Ag loading amounts. (c) Linear-sweep voltammograms of bare Si and Ag-Si electrode with 30 s deposition under various wavelengths irradiation. (d) Current enhancement at -1.0 V at different conditions.

The transient current of Si MWs were measured at -1.0 V under chopped illumination (see Fig. S7, ESI). All Si MW samples showed transient switch-on characteristics under pulsed illumination. Furthermore, the gas evolution of photoelectrodes was measured at -1.0 V under solar irradiation (see Fig. S8, ESI). The hydrogen and oxygen evolution rates of Si-HF were 0.89 and 0.39 μmol/min, but Ag-Si-30 photocathodes achieved 8.3 and 4.0 μmol/min. Besides, the hydrogen and oxygen Faradic efficiency of Si-HF were 50.8% and 44.6%, but Ag-Si microflowers were improved to 75.7% and 73.3%, respectively. This suggests that photogenerated carriers conversion to chemical fuels on Si roots were more efficient after modifying with Ag petals. Additionally, Si MWs uniformly modified by Ag particles (abbreviated to Ag╳Si) were prepared through a thermal reduction method for the photocatalytic comparison of different morphologies (see Fig. S9a-c and details in ESI). The on-set potential of Ag╳Si electrodes were even worse as compared to Si-HF electrode (see Fig. S10a, ESI). The X-ray photoelectron spectroscopy (XPS) of Si 2p region showed that the binding energies of 99.5 eV and 103.5 eV were ascribed from the Si MWs and SiO_2, respectively (see Fig. S11, ESI). This result revealed that the insulating oxide layer generated from the heat treatment of preparing the Ag ╳ Si electrodes, and leaded to the serious recombination. Moreover, the particles uniformly modified-Si MWs reduce the photocurrent because of the poor ion and gas diffusion rates on a rougher surface.[3c] Interestingly, the facile chemical method effectively prevented Si MWs from the oxide layers formation during the deposition of Ag particles. Additionally, Ag particles of Ag-Si electrodes were electron collectors functioned as reducing active sites, and the underlying Si MWs were oxidizing

reaction sites. However, the Ag particles of Ag╳Si electrodes deposited on the oxidizing sites to increase the recombination of photoexcited carriers.[13] Si MWs partially decorated by Pt particles (abbreviated to Pt-Si) were also fabricated by the same facile chemical method to exclude the plasmonic effect (see Fig. S9d-e and details in ESI). Compared to the Si-HF electrode, the on-set potential of Pt-Si MWs were enhanced by the co-catalyst assistance (see Fig. S10b, ESI). It is worth to know that the photocurrent enhancement level of Pt-Si MWs were not significant without the LSPR assistance, as compared to the Ag-Si microflowers.

To analyse the effects of Ag petals on photoresponses of Si roots, linear-sweep voltammograms of Si photoelectrodes were measured at dark condition and various wavelengths of the incident illumination (Fig. 2c). Here, the current enhancement was defined as the current of Ag-Si-30 divided by Si-HF electrode at -1.0 V (Fig. 2d). The dark current of Ag-Si-30 increased to -61 μA/cm^2 at -1.0 V (see Fig. S12, ESI), and this ~5 times enhancement as compared with Si-HF was dominantly caused by the Ag catalytic effect. Under visible light (wavelength > 420 nm) irradiation, the enhancement in photocurrent was ~5 times without the effect from the plasmonic excitation of Ag petals. Interestingly, the current enhancement nonlinearly raised to 6.3 times under solar illumination which resulted from the synergetic effect of the Ag co-catalytic and plasmonic assistance. To further evaluate the effect of the plasmon-induced electromagnetic field on the water splitting efficiency, finite element method (FEM) simulations were established based on the SEM images. The simulated absorption spectrum, which was complementary to the experimental data with plasmonic excitation at ~380 nm and innate Ag absorption at the shorter wavelength (see Fig. S13, ESI). Therefore, two various wavelengths (λ = 380 and 300 nm) of the incident irradiation were selected for the simulation. Top view and cross-sectional electric field intensity maps seperately simulated Ag nanorods on the top cap of Si wire (Fig. 3a and 3c) and nonspheres on the surface side (Fig. 3b and 3d). The electric field intensity of Ag-Si MWs at 380 nm was substantially stronger compared to that at 300 nm. Consequently, we noted that plasmon-induced electric fields instead of the inherent absorption of Si MWs increase the generation probability of charge carriers at the interface which further enhance the photocurrent. It is worth to know that the electric field intensity of Ag nanospheres was weaker with respect to Ag nanorods. This suggests that Ag nanorods partially blocked the incident illumination on underlying smaller Ag nanoparticles, which resulted in the weaker electric field intensity. From these results, we propose that strong spatially non-homogeneous electric fields caused by the LSPR of Ag nanorods effectively reduce the recombination to increase the photoreponse. To further analyse the plasmonic effect on the suppressed recombination, we measured the charge transfer resistance between the electrode and electrolyte by electrochemical impedance spectroscopy (EIS) (see Fig. S14, ESI). The impedance of Ag-Si-30 electrode was conducted at -0.18 V (vs Ag/AgCl), which was corresponded to the on-set potential, under various wavelengths of irradiation. Under solar simulation, the smaller semicircle of Nyquist plots indicated that the faster photoexcited carriers separation occurred in Ag-Si MWs through the plasmonic assistance. Additionally, this result also suggested that the LSPR effect improve the interfacial charge transfer to reduce the recombination of electron-hole pairs. We also investigated incident photon-to-electron conversion efficiency (IPCE) at -1.0 V under various wavelengths (Fig 3e). The IPCE of Si-HF electrode at 300 nm and 380 nm illumination shows slight difference resulted from the absorbing discrepancy at different wavelength. However, the IPCE of Ag-Si mircroflowers at 380 nm reached ~9.10% which was about 3 times higher as compared to 300 nm. Because the low inherent absorption of Si MWs at 380 nm leaded to low amount of photogenerated charge carriers, we suggested the IPCE enhancement of Ag-Si electrode at 380 nm was dominantly contributed from the hot electron injection. The maximum IPCE of Si-HF and Ag-Si electrode were achieved 26.3% and 5.02% at ~650 nm, respectively. Besides, we also arranged the IPCE enhancement which was defined as IPCE of Ag-Si electrode was divided by bare Si (see Fig. S15, ESI). The result revealed that the trend of IPCE enhancement was corresponded to the UV-Vis absorption spectra, and the maximum ratio was achieved at ~380 nm which was corresponded to the wavelength of plasmon excitation.

In summary, we deposited Ag plasmonic particles on the Si MWs through a facile chemical method which prevents the formation of insulating oxide layer during the decorating procedure. The Ag-Si microflowers with less rough surfaces avoided suffering from the low ionic and gas diffusion rates for the PEC measurement. The on-set potential of Ag-Si photocathodes positively shifted ~500 mV as compared with the pristine Si MWs because of the co-catalyst effect. Besides, the photocurrent of Ag-Si electrode was optimized to -35 mA/cm^2 at -1.0 V through Ag synergetic assistance.

The authors gratefully acknowledge the financial support of the Academia Sinica (Contract No. AS 103-TP-A06), Ministry of Science and Technology of Taiwan (Contract No. MOST 102-2745-M-002-005-ASP, MOST 103-2112-M-003-009-MY3 and MOST 100-2112-M-003-009-MY3).

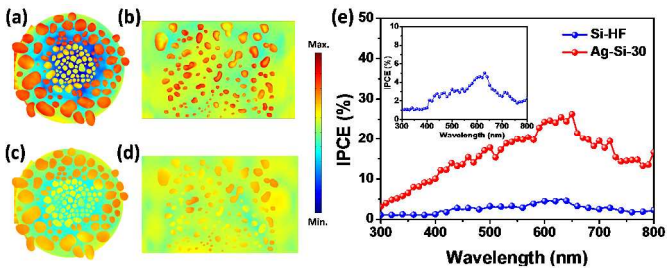

Fig. 3 Top view and cross-sectional electric field intensity maps (in logarithmic scale) of Ag-decorated Si MWs at (a-b) λ = 380 nm and (c-d) λ = 300 nm from FEM simulations. (e) IPCE of pristine Si and Ag-Si electrode with 30 s deposition at different wavelength irradiations (at -1.0 V).

Notes and references

[a] *Department of Chemistry, National Taiwan University, Taipei 106, Taiwan. Email: rsliu@ntu.edu.tw Fax:+886-2-33668671; Tel: +886-2-33661169*
[b] *Department of Physics, National Taiwan Normal University, Taipei 116, Taiwan. Email: sfhu.hu@ntnu.edu.tw Fax:+886-2-29326408; Tel: +886-2-77346079*
[c] *Graduate Institute of Applied Physics, National Taiwan University Taipei 106, Taiwan and Research Center for Applied Sciences, Academia Sinica, Taipei 115, Taiwan.*
[d] *Department of Mechanical Engineering and Graduate Institute of Manufacturing Technology, National Taipei University of Technology, Taipei 106, Taiwan*

† Electronic Supplementary Information (ESI) available: Detailed synthesis, sample preparation, and experimental methods. See DOI: 10.1039/x0xx00000x

1 A. Fujishima and K. Honda, *Nature* 1972, **238**, 37.
2 (a) C. Liu, N. P. Dasgupta and P. D. Yang, *Chem. Mater.* 2014, **26**, 415; (b) E. L. Warren, H. A. Atwater and N. S. Lewis, *J. Phys. Chem. C* 2014, **118**, 747.
3 (a) J. R. McKone, E. L. Warren, M. J. Bierman, S. W. Boettcher, B. S. Brunschwig, N. S. Lewis and H. B. Gray, *Energ. Environ. Sci.* 2011, **4**, 3573; (b) I. Oh, J. Kye and S. Hwang, *Nano Lett.* 2012, **12**, 298; (c) P.

Dai, J. Xie, M. T. Mayer, X. Yang, J. Zhan and D. Wang, *Angew. Chem. Int. Edit.* 2013, **52**, 11119; (d) Y. Hou, B. L. Abrams, P. C. K. Vesborg, M. E. Bjorketun, K. Herbst, L. Bech, A. M. Setti, C. D. Damsgaard, T. Pedersen, O. Hansen, J. Rossmeisl, S. Dahl, J. K. Norskov and I. Chorkendorff, *Nat. Mater.* 2011, **10**, 434; (e) E. L. Warren, J. R. McKone, H. A. Atwater, H. B. Gray and N. S. Lewis, *Energ. Environ. Sci.* 2012, **5**, 9653; (f) S. W. Boettcher, E. L. Warren, M. C. Putnam, E. A. Santori, D. Turner-Evans, M. D. Kelzenberg, M. G. Walter, J. R. McKone, B. S. Brunschwig, H. A. Atwater and N. S. Lewis, *J. Am. Chem. Soc.* 2011, **133**, 1216.

4 (a) K. Sun, Y. Jing, C. Li, X. Zhang, R. Aguinaldo, A. Kargar, K. Madsen, K. Banu, Y. Zhou, Y. Bando, Z. Liu and D. Wang, *Nanoscale* 2012, **4**, 1515; (b) A. Kargar, K. Sun, Y. Jing, C. Choi, H. Jeong, G. Y. Jung, S. Jin and D. Wang, *Acs Nano* 2013, **7**, 9407; (c) A. Kargar, K. Sun, Y. Jing, C. Choi, H. Jeong, Y. Zhou, K. Madsen, P. Naughton, S. Jin, G. Y. Jung and D. Wang, *Nano Lett.* 2013, **13**, 3017.

5 H. A. Atwater and A. Polman, *Nat. Mater.* 2010, **9**, 205.

6 C. Clavero, *Nature Photonics* 2014, **8**, 95.

7 S. Linic, P. Christopher and D. B. Ingram, *Nat. Mater.* 2011, **10**, 911.

8 H. M. Chen, C. K. Chen, M. L. Tseng, P. C. Wu, C. M. Chang, L.-C. Cheng, H. W. Huang, T. S. Chan, D.-W. Huang, R.-S. Liu and D. P. Tsai, *Small* 2013, **9**, 2926.

9 T. Qiu, X. L. Wu, G. G. Siu and P. K. Chu, *Journal of Electronic Materials* 2006, **35**, 1879.

10 (a) H. Tan, R. Santbergen, A. H. M. Smets and M. Zeman, *Nano Lett.* 2012, **12**, 4070; (b) K. Liu, S. Qu, X. Zhang, F. Tan and Z. Wang, *Nanoscale Research Letters* 2013, **8**.

11 (a) K. Sivula, F. Le Formal and M. Graetzel, *Chemsuschem* 2011, **4**, 432; (b) A. J. Bard, *Journal of Photochemistry* 1979, **10**, 59.

12 H. M. Chen, C. K. Chen, C. J. Chen, L. C. Cheng, P. C. Wu, B. H. Cheng, Y. Z. Ho, M. L. Tseng, Y. Y. Hsu, T. S. Chan, J. F. Lee, R. S. Liu and D. P. Tsai, *ACS Nano* 2012, **6**, 7362.

13 C. Zhen, J. C. Yu, G. Liu and H.-M. Cheng, *Chem. Comm.* 2014, **50**, 10416.

ChemComm

RSCPublishing

COMMUNICATION

table of content

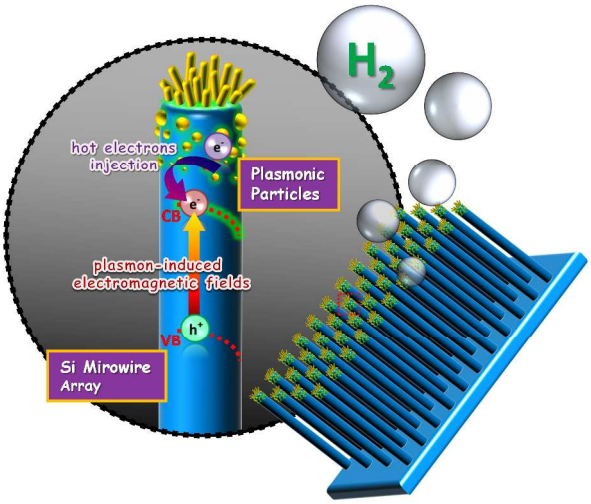

The solar water splitting efficiency of Ag-Si microflowers was enhanced through the synergetic effects of co-catalytic and plasmonic assistance.